Dynamic Study of Field and Current Distribution in Multifilamentary YBCO Thin Films

Francesco Grilli[*,1], Andrea Lucarelli[2], Gunter Lüpke[2], Timothy Haugan[3] and Paul Barnes[3]
[1]Ecole Polytechnique de Montréal, [2]College of William and Mary, [3]Air Force Research Laboratory
*Corresponding author: Ecole Polytechnique de Montréal, P.O. BOX 6079 Station Centre-ville, Montréal (QC), Canada H3C 3A7, f.grilli@polymtl.ca

Abstract: We have developed a model for computing current and field distributions in multifilamentary superconducting thin films subjected to the simultaneous effects of transport ac current and applied dc field perpendicular to the sample. The model is implemented in COMSOL's PDE module (general form) and solves Maxwell equations using a highly non-linear resistivity to describe the superconductor electrical characteristics. The time-dependent magnetic flux and current distribution of multifilamentary thin films are studied for different geometries by changing the distance between the filaments. Our model describes accurately the current and flux dynamics as we would expect from the characterization of real multifilamentary systems. We found that increasing the interfilament distance reduces the coupling and affects the transport and screening current distributions.

Keywords: PDE, Maxwell equations, superconductors, ac losses, thin films.

1. Introduction

The separation of high temperature superconducting (HTS) tapes in filaments is a viable approach to reduce ac losses in HTS high power applications, where ac current and dc field are applied simultaneously [1]. Methods such as mechanical [2], laser scribing [3], photo-lithography [4], or direct printing on buffered substrates using inkjet deposition [5] have been used to create filaments in HTS coated conductors. However, coupling losses between the filaments can overcome the loss reduction due to filamentization at power line frequencies [6]. In order to improve the filamentization process and optimize the ac losses reduction a deep understanding of the flux and current dynamics in multifilamentary HTS in realistic conditions is required. This is a complex nonlinear problem that requires a multiphysics approach since current and field distributions in the superconductor depends strongly on the temperature and the history of the applied field, and transport current. The magnetic flux and current profiles obtained by the finite-element simulations can be directly compared with time-resolved magneto-optical imaging (TRMOI) measurements. The comparison is both a test of the model itself and a source of information on the complex behavior of these systems, as we showed in previous TRMOI studies on HTS single bridged thin films [7]. In this paper we studied the effects of different multifilamentary geometries on the current and field dynamics in the ac regime.

2. Model description

In the work presented in this paper we have neglected the thermal aspects, focusing on the electromagnetic part. This means that the superconductors are considered to be at a constant operating temperature (typically 30 K) and no quenches occur. In addition, since the samples are long and straight, a 2D model considering only the superconducting cross-section is utilized.

The electromagnetic part is described by Faraday's law:

$$\nabla \times \vec{E} = -\frac{\partial \vec{B}}{\partial t}$$

The superconductivity enters the equation by means of the non-linear relation between the electric field and the current density:

$$\rho(J) = \frac{E_c}{J_c}\left|\frac{J}{J_c}\right|^{n-1}.$$

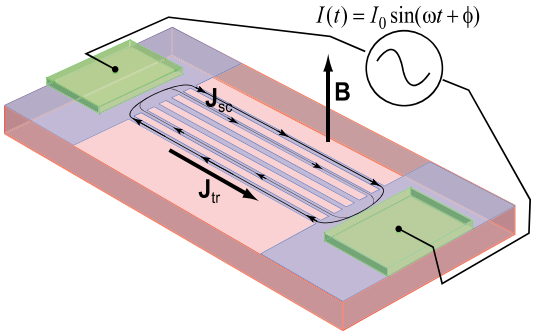

Figure 1. Example of a filamentary YBCO thin film (blue area) grown over an insulating substrate (pink) with metal contact pads (green). The dc field B is applied perpendicularly to the film. The screening currents J_{sc} flow circularly in all the sample. The ac transport current J_{tr} flows along the filaments.

This relation is derived by numerical fits of experimental current-voltage characteristics of superconducting samples. The power index n describes the steepness of the transition from superconducting to normal state and is usually put in relation with the physical phenomena of flux flow and flux creep [8]. As far as the *B-H* constitutive law is concerned, high-temperature superconductors can be simulated by using $B=\mu_0 H$ [9].

The model is implemented in the COMSOL's general PDE module and uses the two magnetic field components as state variables. The use of edge elements of the first order allows having the zero-divergence equation for the magnetic field automatically satisfied. Details about the model implementation can be found in [10]. The external magnetic field is imposed by using Dirichlet boundary conditions in the air domain. The transport current is imposed by using integral constraints in COMSOL's Point Settings. The integral constraints introduce a coupling between the filaments corresponding to the superconductive region connecting the filaments in the real sample (see fig.1).

3. Simulated problem

In our simulations we considered a system made by the air domain and six superconducting filaments 120μm width and 300nm thick connected at the ends. The dimensions chosen for the system correspond to real $YBa_2Cu_3O_{7-x}$ (YBCO) thin films grown by pulsed laser deposition on a $LaAlO_3$ or $SrTiO_3$ substrate and patterned by photolithography to obtain a multifilamentary structure (fig. 1). Since the substrate has very poor conductivity and it is non-magnetic, it has been neglected in the simulated geometry. These films have been previously studied using TRMOI measurements in the same experimental conditions used in the simulations [11]. The chosen external applied field intensity is 5 mT and the ac current $I(t) = I_0 \sin(2\pi f \cdot t)$ amplitude is I_0=8 Amps and its frequency is f=1000 Hz. For the superconductor's material properties, we used $J_c=3\cdot10^{11}$ A/m^2, $E_c=10^{-4}$ V/m and n=25– which are typical values for YBCO films at about 30K. In order to study the effects of the geometry on the current and field distribution we kept the width of filaments 120μm constant and changed the interfilament distance. We simulated three different geometries with filament/interfilament width ratios comparable with the filament/groove ratios of multifilamentary coated conductors found in the literature and corresponding to 8/1, 4/1 and 2/1 [2-6].

In our model there are no restrictions to simulate systems with a larger number of filaments, different dimensions or even different ratios than used in this paper. However, one should consider that the high aspect-ratio of the thin film geometry introduce a large number of nodes that can severely affect the time of calculation especially for systems with a large number of filaments.

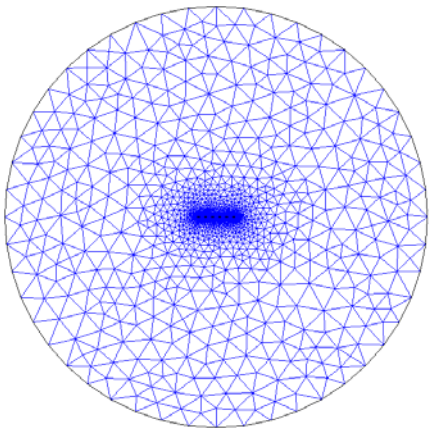

Figure 2. Mesh of the full geometry.

The simulation of two cycles takes about 3-4 hours on a workstation equipped with a 2.4 GHz processor and 3 Gigabytes of RAM. In order to avoid transient effects, three complete cycles of the current in 50 steps were simulated.
An example of the simulated geometry and corresponding mesh is illustrated in figure 2. The circular outer boundary for the air domain is used to impose easily the Dirichlet boundary conditions. The density of nodes in the mesh increases near the filaments as shown in the detailed view of figure 3.

In order to allow direct comparison of the simulations with measurements obtained by techniques sensible to the field dynamics (e.g. Hall probe scanning and arrays, squids, TRMOI, etc.), we extracted the values of the magnetic profile at 1 μm over the sample surface (see fig.3). This method has two effects. To reduce slightly the intensity of the simulated field profiles, similarly to what happens in the real measurements, and to roughen the profiles adding noise due to the coarsening of the mesh. The latter effect could be avoided refining the mesh in that region, but at the cost of an increased calculation time.

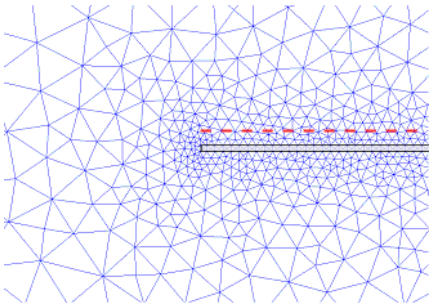

Figure 3. Detailed view of the mesh near the edge of a superconducting filament and pickup level of the simulated field profiles (red dashed line).

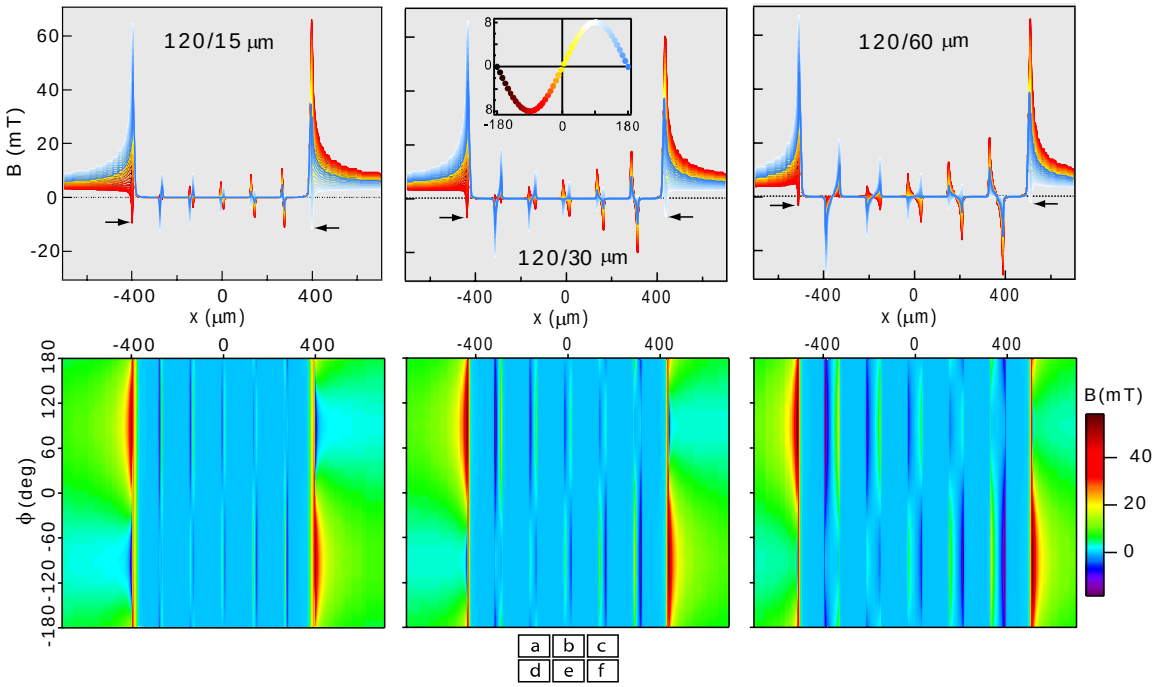

Figure 4. Magnetic field profiles at different phase points and the corresponding time-dependent intensity map for three multifilamentary geometries with filament/groove ratios corresponding to 8/1 (a) and (d), 4/1 (b) and (e), 2/1 (c) and (f).

4. Field dynamics

In figure 4 we present the field profiles at different phase points for the three different geometries adopted in the simulations. We also plotted the intensity of the magnetic field as time-dependent field maps in figure 4 (d),(e) and (f) to represent more clearly the time variations of the field. The magnetic flux partially penetrates into the filaments from the edges forming a front. The flux fronts as well as the flux free regions (Meissner state) in all the filaments remain constant during the cycle for all the three different geometries (fig.4 (a),(b) and (c)). The flux profiles at the edges of the filaments change during the cycle due to the self-field of the applied ac current. The magnetic flux distribution changes also for the three different geometries. Increasing the interfilament distance allows more flux to penetrate in the spacing between the filaments. Here, the peak intensity of the field profiles grows linearly with the spacing (fig.4 (b) and (c)). The flux profiles reach their maximum value of 65 mT at the edges of the two external filaments. The change in the geometry doesn't affect the maximum value of the peaks in the flux profiles, but it changes the dips that forms at the external edges of the sample, indicated by black arrows in figure 4 (a), (b), and (c). This indicates a clear change in the way the sample screens the external magnetic flux for the different geometries. As the interfilament distance increases the screening response is separated into the different filaments and the coupling between the filaments is reduced.

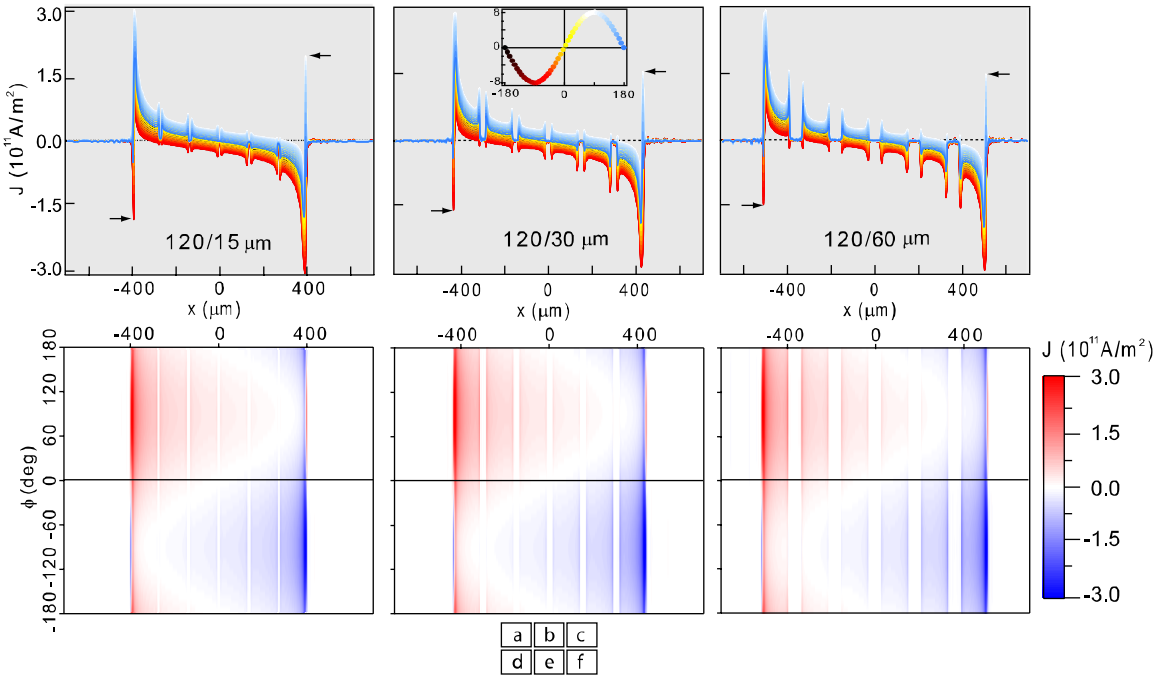

Figure 5. Current density profiles at different phase points and the corresponding time-dependent intensity maps for three multifilamentary geometries with filament/groove ratios corresponding to 8/1 (a) and (d), 4/1 (b) and (e), 2/1 (c) and (f).

5. Current Dynamics.

The current dynamics provides additional useful information regarding the effects of the geometry on the coupling between the filaments. Figure 5 shows the field profiles at different phase points and the corresponding time-dependent field maps. The maps show at a first glance how the current in each filament changes sign during the cycle, from positive (red) passing through zero (white) to negative (blue). Interestingly a "return current" of opposite sign (black arrows in figure 5 (a),(b) and (c)) flows in a narrow region at the edges of the left external filament on the first half of the cycle ($-180°<\phi<0°$) and on the right external filament on the second half ($-180°<\phi<0°$). This current causes the steep variation from positive to negative flux observed in the same region for the field profiles (fig. 4). A similar behavior has been observed in TRMOI measurements of single bridged YBCO thin films [12]. The return current is reduced by increasing the spacing between the filaments from the geometry 120/15 to 120/60. The increased distance reduces the coupling between the filaments and redistributes the screening currents between the filaments. The growth of the peak intensity at the edges of all the filaments is a further indication of the reduced coupling between the filaments. For the three different geometries the current density in the two external filaments shows the most intense value corresponding to the critical current density $J_c=3\cdot10^{11}$ A/m^2, as predicted by the critical state model. This result represents further proof of the accuracy of our method.

The current density profiles shown in figure 5 were obtained from the field profiles by inversion of the Biot-Savart law. This method has some limitations, as

discussed in paragraph 3, but it allows direct comparison of the simulated results with experimental measurements. The current profiles obtained by the inversion method differ only slightly from those calculated directly by the COMSOL model. Our method does not change the overall shape of the current profiles, neither does it affect their time-dependent behavior, but it smoothes and partially reduces the intensity of the peaks.

In figure 6 we show the integrated current densities at different phase points and the best fit for the three simulated geometries. The screening component of the current is symmetric, as shown by the field profile (fig. 4) and the current profile (fig. 5) at ϕ=-180°, ϕ=0° and ϕ=180°. Thus, in the integration of the current density over all the filaments the screening current is cancelled out and we obtain the total transport current. Figure 6 shows that the amplitude and phase of the total transport current are not affected by the change in the geometry. This quantitative analysis also confirms that the reduction of the current intensity introduced by our inversion method is less than 1.3%.

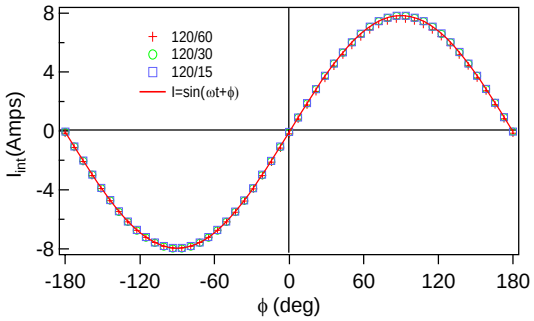

Figure 6. Total current flowing in all the filaments calculated at different phase points for the three different geometries (symbols) and best fit (solid line).

Figure 7 shows the transport current per filament for the three different geometries. Only the first three filaments are represented for clarity. The behavior of the other three filaments is completely symmetric. The current flows in each filament without any significant shift in the phase with respect to the applied current. Most of the current flows in the external filaments for all the geometries. The 120/60 geometry shows higher values of the current in the internal filaments but lower values for the external ones as compared to the other two geometries. As the distance between the filament is increased the transport current distributes more evenly between the filaments. The total transport current does not change (figure 6), but the geometry affects the transport current distribution due to the coupling between the filaments, as we also observed for the field distribution.

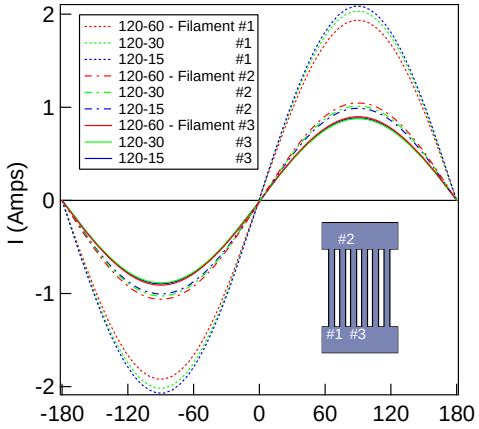

Figure 7. Transport current per filament for the first three filaments (inset) for the three different geometries.

6. Conclusions.

We studied the field and current dynamics of a multifilamentary superconducting thin film by numerical simulation using the COMSOL's PDE module (general form) to solve Maxwell's equations. We used a highly non-linear resistivity to describe the electrical characteristics of the superconducting film. The model has been developed to compare directly the simulations with the measurements of real systems performed by

experimental techniques sensible to the local magnetic field variations such as Hall probe scanning and arrays, squids, TRMOI. We observed that an increased interfilament distance produces a change in the field and current dynamics due to the reduced coupling between the filaments. The screening and transport current redistribute more evenly between all the filaments that respond more independently to the applied field and ac current.

7. References

1. W.J. Carr, C.E. Oberly, *IEEE Trans. Applied Superconductivity*, **vol. 9**, no. 2, pp. 1475-1478 (1999).
2. S.P. Ashworth, F. Grilli, *Supercond. Sci. Tech.*, **vol. 19**, pp. 227-232, (2006).
3. M. Majoros, B. A. Glowacki, A M. Campbell, G. A. Levin, P. N. Barnes, M. Polak, *IEEE Trans. Appl. Supercond.*, **vol. 15**, no. 2, pp. 2819-2822, (2005).
4. D.W. Hazelton et al., *Advances in Cryogenic Enginering-ICMC*, vol. 52, pp. 859-868, (2006).
5. R.C. Duckworth et al., *IEEE Trans. Appl. Supercond.*, **vol. 17**, no. 2, pp. 3159-3162 (2007).
6. M.D. Sumption, E.W. Collings, P.N. Barnes, *Supercond. Sci. Tech.*, **vol. 18**, pp. 122-134 (2005).
7. A. Lucarelli, et al Applied Physics A, **vol. 88**, (2007) pp. 601-604
8. R.P. Huebener, *Magnetic Flux Structures in Superconductors* 2nd edn., pp. 245-251, Springer, Berlin; New York, (2001).
9. J. Paasi, M. Lahtinen, Physica C, **vol. 310**, pp. 57-61 (1998).
10. R. Brambilla, F. Grilli, L. Martini. *Superconductor Science and Technology*, **vol. 20**, pp. 16-24 (2007).
11. A comparison of simulated and measured TRMOI data will be published elsewhere.
12. A. Lucarelli, et al. *Superconductor Science and Technology*, in print Nov. (2008).

8. Acknowledgements

This work was supported by the Mathematics of Information Technology and Complex System (MITACS) network. The work at CWM is supported by the DOE grant DEFG02-04ER46127.